Journal of Materials Chemistry C

ROYAL SOCIETY OF CHEMISTRY

PAPER

View Article Online
View Journal | View Issue

Cite this: J. Mater. Chem. C, 2022, 10, 13905

n-Type conjugated polymers comprising bithiophene imide and multifluorinated thiophene moieties synthesized by direct arylation polycondensation†

Houji Cai,[a] Xuwen Zhang,[a] Yibo Shi,[a] Chenhui Xu,[a] Tianzuo Wang,[a] Cheng Wang,[a] Tian Du,[a] Yunfeng Deng *[a] and Yanhou Geng [ab]

Received 22nd February 2022,
Accepted 3rd June 2022

DOI: 10.1039/d2tc00732k

rsc.li/materials-c

We synthesized four n-type conjugated polymers comprising a bithiophene imide (BTI) unit and 3,3′,4,4′-tetrafluoro-2,2′-bithiophene (4FBT) or (*E*)-1,2-bis(3,4-difluorothien-2-yl)ethene (4FTVT) *via* direct arylation polycondensation, and comprehensively studied the optical, electrochemical and charge transport properties of the polymers. Increasing the BTI acceptor unit from one to two in the repeating unit slightly decreased the frontier molecular orbital levels of the polymers and blue-shifted their absorption spectra. Moreover, this change altered the molecular packing from an edge-on backbone orientation to bimodal packing with mixed edge-on and face-on orientations. When used as semiconductor layers in organic thin-film transistors, all four polymers exhibited unipolar n-type transport behavior with the highest saturation and a linear electron mobility of 0.72 and 0.67 $cm^2 V^{-1} s^{-1}$, respectively. Our findings suggest that direct arylation polycondensation can serve as an ecofriendly protocol for the synthesis of high-performance n-type conjugated polymers based on BTI through careful molecular design.

Introduction

Conjugated polymers (CPs) have attracted much attention owing to their potential utility for the fabrication of low-cost, lightweight organic electronics, such as organic thin-film transistors (OTFTs).[1–5] In the last two decades, remarkable progress has been achieved in the development of high-performance CPs. However, most of the polymers reported to date exhibit p-type behavior, and the development of n-type CPs has lagged behind.[6–14] Since p-type and n-type materials are essential for organic devices, it is imperative to develop high-performance n-type CPs.[7,8,12,13]

Constructing donor–acceptor (D–A) type CPs is an effective and widely used approach to develop high-performance CPs.[1,15–20] However, the incorporation of an electron-rich D unit can increase the energy of the highest occupied molecular orbital (E_{HOMO}), resulting in D–A CPs that tend to exhibit p-type or ambipolar transport characteristics.[13,21] To address this issue, a strategy of constructing CPs with a strong A unit and a weak D unit (SA–WD) has been developed.[13,22] Weak D units are generally obtained by incorporating electron-withdrawing groups, such as fluorine atoms (F) or cyano groups (CN), into the electron-rich moieties. The extra electron-withdrawing groups on the D unit can simultaneously lower both E_{HOMO} and the energy of the lowest unoccupied molecular orbital (E_{LUMO}) of the CPs, thus facilitating electron injection and

[a] School of Materials Science and Engineering and Tianjin Key Laboratory of Molecular Optoelectronic Science, Tianjin University, Tianjin 300072, P. R. China. E-mail: yunfeng.deng@tju.edu.cn
[b] Joint School of National University of Singapore and Tianjin University, International Campus of Tianjin University, Fuzhou 350207, China

† Electronic supplementary information (ESI) available. See DOI: https://doi.org/10.1039/d2tc00732k

Yunfeng Deng

Yunfeng Deng received his PhD degree in Polymer Chemistry and Physics from Changchun Institute of Applied Chemistry, Chinese Academy of Sciences in 2015. He then joined University of Waterloo and Technion-Israel Institute of Technology as a postdoctoral research fellow. Currently, he is an associate professor in the School of Materials Science and Engineering, Tianjin University, China. His research mainly focuses on the design and synthesis of conjugated materials and their related electronic devices.

suppressing hole accumulation. Various n-type CPs have been reported by means of the SA–WD approach.[21,23–31] For example, Guo and coworkers synthesized a bithiophene imide (BTI)-based SA–WD-type polymer by using difluorothiophene as a weak D unit; the resulting polymer showed unipolar n-type transport characteristics with an electron mobility (μ_e) of 1.13 $cm^2\ V^{-1}\ s^{-1}$.[29] Hwang and coworkers copolymerized a thiophene-flanked diketopyrrolopyrrole unit with a CN-substituted thiophene–vinylene–thiophene unit to obtain a SA–WD-type polymer with a μ_e value of $>1.0\ cm^2\ V^{-1}\ s^{-1}$.[23] However, most of these polymers were synthesized by Stille polycondensation, which requires an additional step to synthesize an organotin monomer and produces stoichiometric quantities of highly toxic waste.[32–34]

Direct arylation polymerization (DArP) has emerged as a promising protocol for synthesizing CPs.[35–39] This method allows the formation of carbon–carbon bonds between (hetero)arenes and (hetero)aryl halides, thus avoiding the need for organotin reagents and the generation of toxic side products. To date, most of the high-performance CPs are derived from thiophene-based monomers. Because of the low selectivity between α-C–H and β-C–H bonds in thiophene, side reactions such as branching and cross-linking may occur during DArP, especially when the polymerization is performed in a polar aprotic solvent.[34,37,40–43] These side reactions will lead to structural defects that severely erode the performance of CPs. In view of this challenge, it is not surprising that only a limited number of high-performance CPs have been synthesized by DArP.[21,32,44–56] Recently, we developed two weak D units, 3,3′,4,4′-tetrafluoro-2,2′-bithiophene (4FBT) and (*E*)-1,2-bis(3,4-difluorothien-2-yl)ethene (4FTVT), by installing F atoms at the β-positions of the thiophene rings. Both 4FBT and 4FTVT show high reactivity and selectivity in DArP. In addition, the weak intramolecular F···S interactions endow the resulting polymer backbones with good planarity. As a consequence, high-performance CPs can be synthesized *via* DArP with these two units.[21,53,54,56] In the current study, we synthesized four SA–WD-type polymers, designated P(BTI-4FBT), P(BTI-4FTVT), P(BTI2-4FBT), and P(BTI2-4FTVT), *via* DArP with dibrominated BTI (BTI-2Br) or its dimer (BTI2-2Br) as the C–Br monomer and 4FBT or 4FTVT as the C–H monomer (Fig. 1). By comparing the properties of BTI- and BTI2-based polymers, the effect of adding a second BTI acceptor unit was studied. We found that increasing the number of acceptors in the polymer repeat unit decreased the frontier molecular orbital levels and increased the electron mobility of the polymers. All four polymers showed n-type transport characteristics in OTFT devices, with a maximum μ_e of 0.72 $cm^2\ V^{-1}\ s^{-1}$. Notably, the μ_e values extracted from the saturation and linear regimes were almost the same, indicating that the reported mobilities are highly reliable.

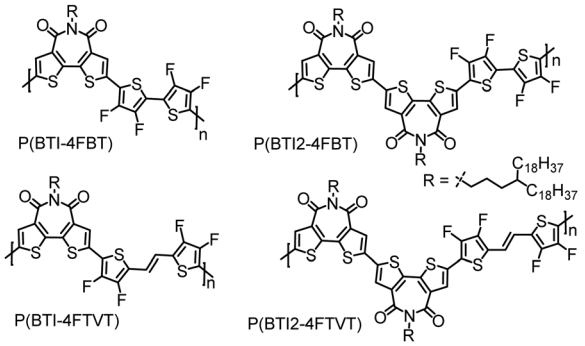

Fig. 1 Chemical structures of the polymers.

Results and discussion

Design and synthesis

BTI was selected as the A unit because of its strongly electron-withdrawing character, easy access, and the solubilizing capability of the imide moiety. Additionally, differing from naphthalene diimide, the BTI unit can mitigate backbone torsion, which was expected to result in a more planar polymer backbone and thus in enhanced charge transport.[9,57,58] It was reasonable to suppose that incorporating a BTI2 unit into the polymer backbone would increase the density of the A unit, allowing us to further tune the frontier molecular orbital levels of the CPs.[59–62] To increase the solubility of the polymers, while retaining close π–π stacking, we used long and distantly branched 4-octadecyldocosyl groups as the side chains.

The syntheses of the monomers and polymers are shown in Scheme 1. Compound **4**, 4FBT, and 4FTVT were prepared according to previously reported procedures.[53,54,63] *N*-Substituted phthalimide **2** was prepared from alcohol **1** using a Mitsunobu reaction and was then converted to alkyl amine **3** by hydrazinolysis (68% yield for two steps). BTI was synthesized by the reaction of compounds **3** and **4** in a yield of 96%, which can be readily brominated with Br_2 to give the dibrominated monomer BTI-2Br (75%) or monobrominated BTI (BTI-Br, 20%) in the presence of a catalytic amount of ferric chloride ($FeCl_3$). BTI2 was obtained in an 80% yield from BTI-Br by a $Pd(PPh_3)_4$-catalysed one-pot Stille homocoupling reaction with

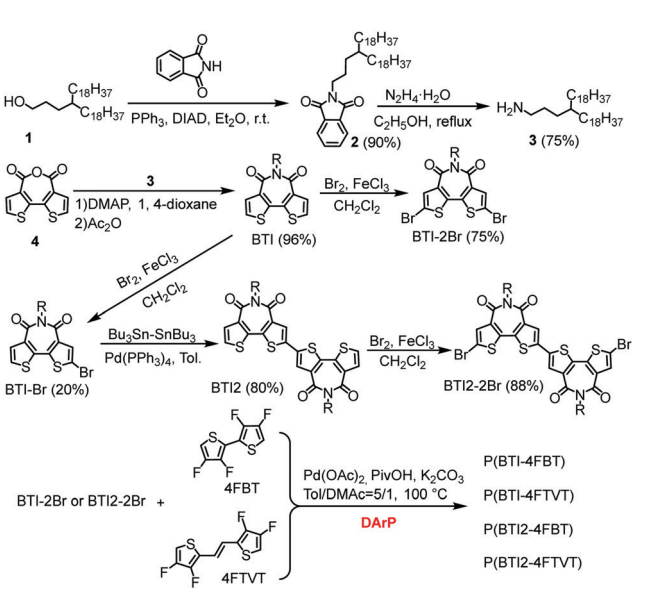

Scheme 1 Syntheses of the monomers and polymers.

hexamethyldistannane and was subsequently brominated with Br_2/$FeCl_3$ to afford dibrominated monomer BTI2-2Br in an 88% yield.

We initially attempted the DArP reaction by using Herrmann's catalyst with P(*o*-OMePh)$_3$ as a ligand in the presence of pivalic acid and Cs_2CO_3; this combination has been used for the synthesis of high-molecular-weight CPs with isoindigo and diketopyrrolopyrrole derivatives as C–Br monomers.[21,53,54,56] However, this condition only caused oligomer formation (Table S1, ESI†). A combination of $Pd_2(dba)_3{\cdot}CHCl_3$ and P(*o*-MeOPh)$_3$ gave a similar result. Alternatively, CPs with high molecular weights could be obtained under phosphine-free conditions with $Pd(OAc)_2$ as the catalyst and K_2CO_3 as the base in a mixture of toluene and dimethylacetamide (DMAc). Considering that DMAc is not a good solvent for the polymer, the DMAc content was then optimized. It was found that the best result was achieved with 20 vol% DMAc in toluene. Under the optimal conditions, P(BTI-4FBT), P(BTI-4FTVT), P(BIT2-4FBT), and P(BTI2-4FTVT) were obtained in yields of >90% with number-average molecular weights (M_ns) of 20.5, 19.0, 37.4, and 47.7 kDa, respectively. The molecular weights of the polymers were measured by high-temperature gel permeation chromatography at 150 °C after purification by successive Soxhlet extractions (Fig. S1, ESI†). The much lower M_ns of P(BTI-4FBT) and P(BIT-4FTVT) relative to those of P(BTI2-4FBT) and P(BTI2-4FTVT) may be attributable to their low solubility induced by the low density of solubilizing alkyl chains. In fact, the solutions of P(BTI-4FBT) and P(BTI-4FTVT) jelled during the polymerization reactions. All the polymers showed good solubility in warm chlorobenzene and *o*-dichlorobenzene (*o*-DCB). We believe that the optimal DArP conditions developed in this work may also be applicable to other BTI derivatives. Thermogravimetric analysis (TGA) revealed that all the polymers show good thermal stability with decomposition temperatures exceeding 380 °C (Fig. S2, ESI†). A thermal transition due to melting of the long alkyl chains was observed in the differential scanning calorimetry (DSC) profiles of the polymers (Fig. S3, ESI†).[56,64] Interestingly, the transition temperatures and enthalpy changes of BTI2-based polymers are higher than those of BTI-based polymers. This phenomenon may be attributed to their different alkyl chain densities, which could affect the interdigitation of the alkyl chains and their lamellar stacking.

Density functional theory calculations

To understand the effects of F introduction and dual A units on the properties of the polymers, DFT calculations were performed on the trimeric models at the B3LYP/6-31G(d,p) level using the Gaussian 09 program. For comparison, calculations were also performed for polymers without F atoms, that is, P(BTI-BT) and P(BTI-TVT). The optimized trimer conformations for the 4FBT- and 4FTVT-based polymers are shown in Fig. 2 and Fig. S4 (ESI†), respectively. As expected, the calculated E_{HOMO} and E_{LUMO} of P(BTI-4FBT) were lower than those of the parent polymer P(BTI-BT). Increasing the density of the BTI unit lowered E_{HOMO} and E_{LUMO} even further. In addition, the introduction of F atoms also increased the planarity of the polymer backbone. The dihedral angle between BTI and the bithiophene moiety in P(BTI-BT) was 9.2°, which gave P(BTI-BT) a slightly twisted geometry. In contrast, the corresponding dihedral angles for P(BTI-4FBT) and P(BTI2-4FBT) were only 0.7° and 0.1°, respectively, owing to the presence of noncovalent intramolecular F···S interactions. As shown in Fig. 2, the calculated F···S distance (2.95 Å) was shorter than the sum of the van der Waals radii of F and S (3.27 Å), suggesting an F···S interaction.[65] Similar trends were found for the 4FTVT-based polymers (Fig. S4, ESI†).

Optical and electrochemical properties

Solution and thin-film UV-vis-NIR absorption spectra of the four polymers are shown in Fig. 3, and the corresponding data are summarized in Table 1. In dilute *o*-DCB solution, each polymer showed an absorption peak with a pronounced shoulder. Compared with the 4FBT-based polymers, the 4FTVT-based polymers showed solution absorption maxima (λ_{max}^{sol}) that were bathochromically shifted by *ca.* 20 nm because the 4FTVT unit is more electron rich than the 4FBT unit. Increasing the BTI loading resulted in a blue shift of the λ_{max}^{sol}, particularly for the 4FTVT-based polymers, which showed a blue shift of 7 nm. The profiles of the thin-film absorption spectra were similar to those of the solution spectra and there was little difference between the λ_{max} values for the solution and thin-film spectra, suggesting that some preaggregation of these polymers occurred in solution.[66,67] This statement can be

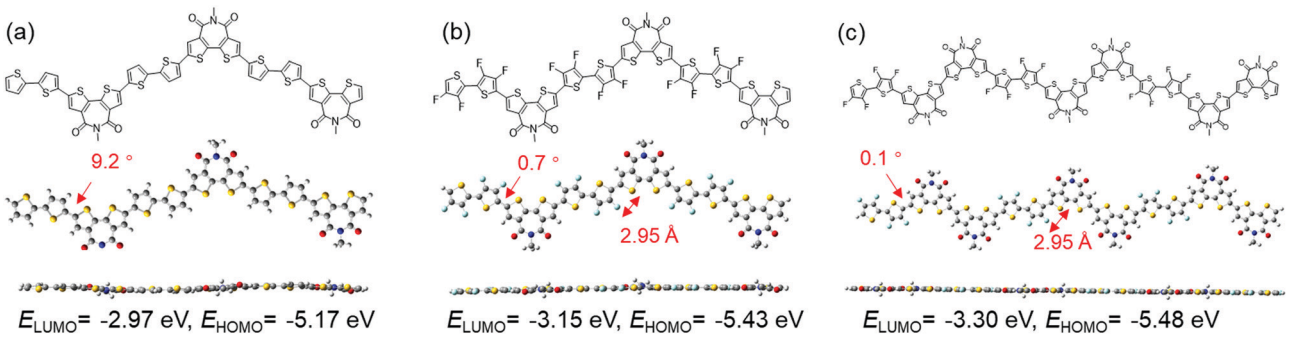

Fig. 2 Optimized molecular geometries and energy levels for (a) P(BTI-BT), (b) P(BTI-4FBT), and (c) P(BTI2-4FBT) trimers. Calculations were performed at the B3LYP/6-31G(d,p) level; the alkyl chains were replaced with methyl groups to simplify the calculations.

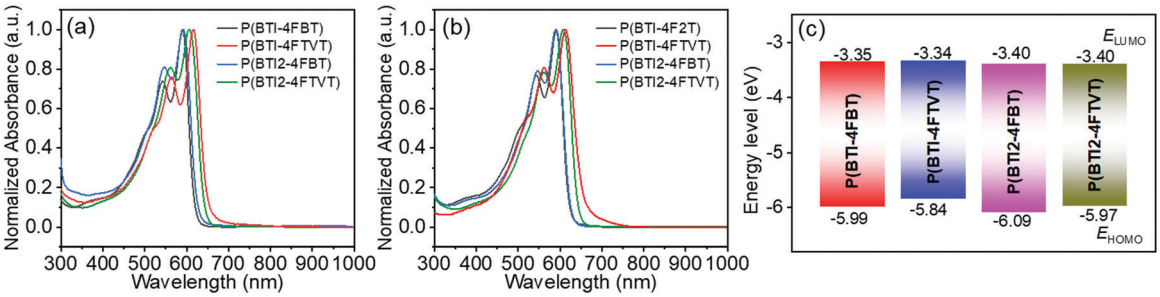

Fig. 3 (a) Solution and (b) thin-film UV-vis-NIR absorption spectra and (c) energy level diagrams of the polymers. Solution spectra were measured in *o*-DCB with a concentration of 10^{-5} mol L^{-1} of the repeating units. Thin films were prepared by spin-coating the *o*-DCB solutions on quartz substrates. E_{HOMO} and E_{LUMO} values were estimated from the redox onsets in the thin-film cyclic voltammetry curves.

Table 1 Molecular weights, optical properties, and energy levels of the polymers

Polymer	M_n [kDa]	$Đ$	T_d[a] [°C]	λ_{max}^{sol} [nm]	λ_{max}^{film} [nm]	E_g^{opt}[b] [eV]	E_{HOMO}[c] [eV]	E_{LUMO}[c] [eV]
P(BTI-4FBT)	20.5	2.1	381	592	592	1.97	−5.99	−3.35
P(BTI-4FTVT)	19.0	3.2	403	615	615	1.86	−5.84	−3.34
P(BTI2-4FBT)	37.4	2.1	407	590	590	1.99	−6.09	−3.40
P(BTI2-4FTVT)	47.7	2.4	428	608	607	1.90	−5.97	−3.40

[a] 5% weight loss temperature. [b] Optical band gaps were calculated from the thin-film absorption onsets: $E_g^{opt} = 1240/\lambda_{onset}$. [c] E_{HOMO} and E_{LUMO} were calculated as follows: $E_{HOMO} = -(4.40 + E_{onset}^{ox})$ eV and $E_{LUMO} = -(4.40 + E_{onset}^{re})$ eV, where E_{onset}^{ox} and E_{onset}^{re} are the oxidation and reduction onset potentials of the polymers *versus* SCE.

further supported by the variable-temperature UV-vis-NIR spectra (Fig. S5, ESI†), in which λ_{max} was gradually blue-shifted as the temperature was increased from 20 to 90 °C. The optical band gaps (E_g^{opt}) calculated from the thin-film absorption onsets for P(BTI-4FBT), P(BTI-4FTVT), P(BTI2-4FBT), and P(BTI2-4FTVT) were 1.97, 1.86, 1.99, and 1.90 eV, respectively.

Film cyclic voltammetry (CV) measurements were performed to characterize the electrochemical properties of the four polymers. The E_{HOMO} and E_{LUMO} of the polymers were estimated from the onsets of the oxidation and reduction peaks, respectively. All the polymers displayed obvious redox peaks (Fig. S6, ESI†). The E_{LUMO}s and E_{HOMO}s of P(BTI-4FBT), P(BTI-4FTVT), P(BTI2-4FBT), and P(BTI2-4FTVT) were −3.35 and −5.99, −3.34 and −5.84, −3.40 and −6.09, and −3.40 and −5.97 eV, respectively. In comparison, previously reported BTI-based polymer analogues without F atoms showed E_{LUMO} and E_{HOMO} of −3.22 and −5.45 eV;[68] P(BTI-4FBT) exhibited lower E_{HOMO} and E_{LUMO} and the difference between the E_{HOMO} was particularly pronounced. A lower E_{HOMO} is highly desirable for realizing unipolar n-type transport because it is beneficial for blocking hole injection.[13] Switching from 4FBT to 4FTVT almost had no effect on the E_{LUMO}s but increased the E_{HOMO}s. In contrast, increasing the number of BTI units in the repeating unit decreased both E_{HOMO} and E_{LUMO}.

Charge transport properties of the polymers

The charge-transport properties of the four polymers were investigated by fabricating OTFT devices with a top-gate bottom-contact (TGBC) device configuration. All the polymers showed n-type transport properties, but the threshold voltage (V_T) is very high (>50 V) (Fig. S7, ESI†). The large V_T is attributed to the high electron injection barrier between the polymer LUMO energy level and electrode Fermi level.[69] In order to facilitate electron injection, an ultrathin polyethylenimine ethoxylate (PEIE) was inserted between the source/drain electrodes and polymer thin film.[70,71] The PEIE-modified device performance parameters, electron mobility ($\mu_{e,sat}$ and $\mu_{e,lin}$), current on/off ratio (I_{on}/I_{off}), and V_T are summarized in Table 2. Representative transfer characteristics, output characteristics, and the gate–source-voltage (V_{GS})-dependence of the mobility of the OTFT devices are shown in Fig. 4. Almost no hysteresis was observed in the transfer and output curves. The relatively high off current was probably due to the weak contact doping of the polymers by PEIE treatment.[72] Previous studies have shown that BTI-bithiophene copolymers exhibit p-type or ambipolar transport characteristics.[63,68] In contrast, P(BTI-4FBT), P(BTI-4FTVT), P(BTI2-4FBT), and P(BTI2-4FTVT) showed unipolar n-channel transistor behaviour. This behavior can be ascribed to the low E_{HOMO}s of the polymers, which efficiently blocked hole injection from the gold electrode. P(BTI-4FBT)

Table 2 Performance of the polymer-based OTFT devices[a]

Polymer	$\mu_{e,sat}$[b] [$cm^2\ V^{-1}\ s^{-1}$]	$\mu_{e,lin}$[b] [$cm^2\ V^{-1}\ s^{-1}$]	V_T [V]	I_{on}/I_{off}
P(BTI-4FBT)	0.19 (0.17)	0.16 (0.14)	13 ± 2	~10^5
P(BTI-4FTVT)	0.30 (0.28)	0.27 (0.24)	15 ± 3	~10^5
P(BTI2-4FBT)	0.40 (0.35)	0.35 (0.32)	11 ± 2	~10^5
P(BTI2-4FTVT)	0.72 (0.65)	0.67 (0.60)	10 ± 2	~10^5

[a] The source–drain electrodes were modified with 0.04 wt% PEIE before deposition of the polymer semiconductor, and the polymer thin films were annealed at 150 °C for 30 min in an argon atmosphere. [b] Mobilities were measured under ambient conditions; average values are in parentheses.

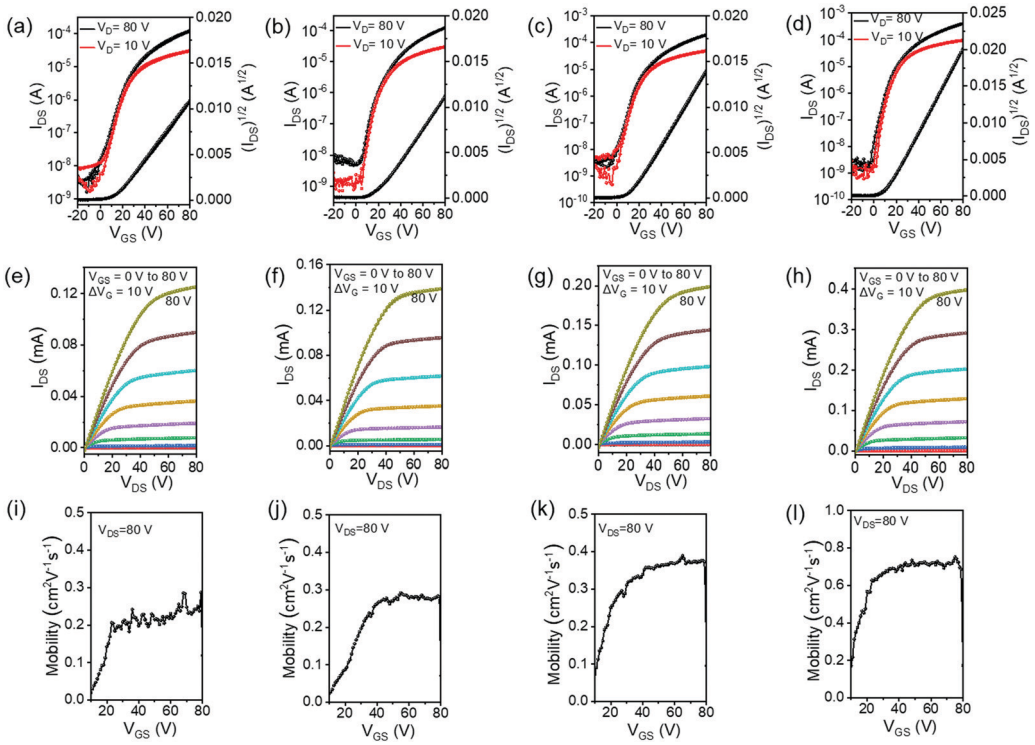

Fig. 4 Typical (a–d) transfer curves, (e–h) output curves, and (i–l) saturation mobility *versus* V_{GS} curves of the PEIE modified TGBC OTFT devices based on (a, e and i) P(BTI-4FBT), (b, f and j) P(BTI-4FTVT), (c, g and k) P(BTI2-4FBT), and (d, h and l) P(BTI2-4FTVT). Thin films of the polymers were prepared from *o*-DCB solutions and were annealed at 150 °C for 30 min in an argon atmosphere.

showed a $\mu_{e,sat}$ of 0.19 cm^2 V^{-1} s^{-1}. TVT has a more rigid and planar skeleton than BT,[21,56] and therefore P(BTI-4FTVT) displayed a higher $\mu_{e,sat}$ (0.30 cm^2 V^{-1} s^{-1}). Insertion of an additional BTI unit into the repeating unit further increased the $\mu_{e,sat}$: P(BTI2-4FBT) and P(BTI2-4FTVT) showed $\mu_{e,sat}$ of 0.40 and 0.72 cm^2 V^{-1} s^{-1}, respectively. Note that the $\mu_{e,sat}$ were obtained from the well linear $(I_{DS})^{1/2}$ *versus* V_{GS} curves, and comparable μ_e were extracted from the saturation and linear regimes, unambiguously demonstrating the reliability of the device performance.[73,74] The reliability was also supported by the weak dependence of mobility on gate voltage (Fig. 4i–l).

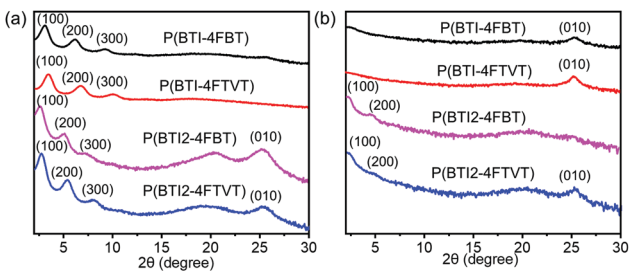

Fig. 5 (a) Out-of-plane and (b) in-plane X-ray diffraction profiles of the polymer thin films. The films were annealed at 150 °C for 30 min in an argon atmosphere.

Film microstructures and morphology

Grazing incidence X-ray diffraction (XRD) and tapping-mode atomic force microscopy (AFM) were employed to study the microstructures and morphology of the polymer thin films. P(BTI-4FBT) and P(BTI-4FTVT) featured pronounced lamellar diffractions progressing up to (300) in the out-of-plane direction. Meanwhile, a (010) peak corresponding to π–π stacking was observed in the in-plane direction (Fig. 5). These results indicate that P(BTI-4FBT) and P(BTI-4FTVT) adopted an edge-on orientation. Intriguingly, BTI2-based polymers showed a different packing texture. Except for the out-of-plane reflections of up to the third order (300), additional out-of-plane (010) and in-plane (100) and (200) peaks appeared (Fig. 5), indicating that these two polymers adopted a bimodal packing with mixed edge-on and face-on orientations of the polymer chains. This packing model is beneficial for charge carrier transport because the parallel and perpendicular orientations of the π-stacking planes can form three-dimensional conduction channels. A detailed investigation of bimodal orientation leading to enhanced charge transport in other CPs is reported.[75–78] In comparison to P(BTI2-4FBT), P(BTI2-4FTVT) showed an obvious in-plane (010) peak, implying that it had higher-order packing. The lamellar *d*-spacings calculated from the out-of-plane (100) diffraction peaks were 28.4 and 26.0 Å for P(BTI-4FBT) and P(BTI-4FTVT), respectively. Increasing the number of BTI units enlarged the lamellar *d*-spacings to 35.1 and 32.7 Å for P(BTI2-4FBT) and P(BTI2-4FTVT), respectively. All four polymers showed a π–π stacking distance of *ca.* 3.52 Å, as calculated from the (010) diffraction peak. Collectively, the bimodal backbone orientation and high-order packing in the

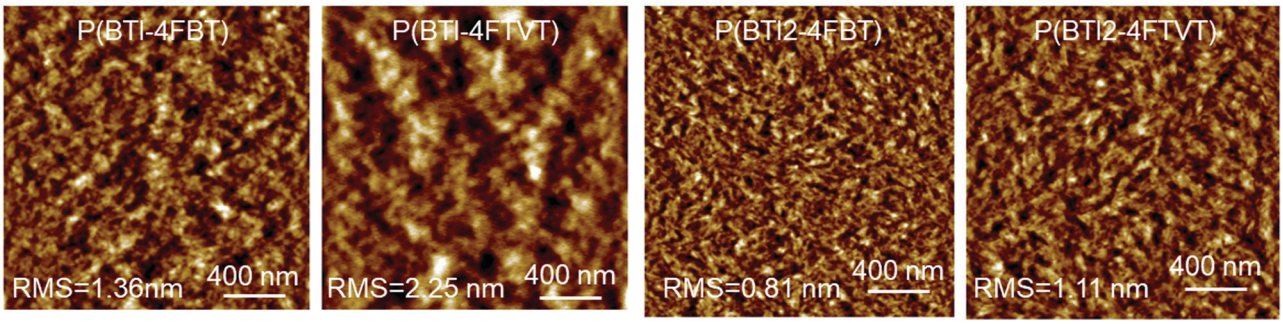

Fig. 6 Atomic force microscopy height images (2 μm × 2 μm) of polymer thin films. The films were annealed at 150 °C for 30 min in an argon atmosphere.

thin film synergistically contributed to the high mobility of P(BTI2-4FTVT).

AFM height images of the polymer thin films after thermal annealing at 150 °C for 30 min are shown in Fig. 6. All the films were continuous and smooth with root-mean-square (rms) roughness values of 0.81–2.25 nm and the films were characterized by a fibre-like morphology. However, the fibre-like nanostructures of P(BTI2-4FBT) and P(BTI2-4FTVT) were more obvious, which is consistent with the fact that P(BTI2-4FBT) and P(BTI2-4FTVT) showed higher mobilities than P(BTI-4FBT) and P(BTI-4FTVT).

Conclusions

In summary, we synthesized four n-type CPs, *i.e.* P(BTI-4FBT), P(BTI-4FTVT), P(BTI2-4FBT), and P(BTI2-4FTVT), *via* DArP using BTI or BTI2 as the C–Br monomer and 4FBT or 4FTVT as the C–H monomer. All four polymers showed planar backbones owing to the presence of F···S intramolecular noncovalent interactions. Increasing the number of BTI units in the repeating unit decreased both the E_{LUMO} and E_{HOMO} of the polymers. This change also had a pronounced effect on the thin-film microstructures and morphology and consequently on the charge-carrier transport performance. Unipolar n-channel OTFTs were fabricated with these four polymers as the semiconductor layers. Of the polymers, P(BTI2-4FTVT) delivered the best device performance, with maximum saturation and linear μ_e of 0.72 and 0.67 $cm^2\ V^{-1}\ s^{-1}$, respectively. The high mobility of P(BTI2-4FTVT) can be attributed to its bimodal backbone orientation, high-order packing in the thin film, and favorable thin-film morphology. This work demonstrates that high-mobility n-type CPs can be synthesized by means of DArP, an atom-economical and ecofriendly protocol, through careful selection of the co-monomer.

Conflicts of interest

There are no conflicts to declare.

Acknowledgements

This work was supported by the National Key R&D Program of China (2021YFA0717900), National Natural Science Foundation of China (no. 52073209) and Tianjin Natural Science Foundation (no. 19JCYBJC18100). In addition, Y. Deng would like to thank the Peiyang Scholar Program of Tianjin University for support.

Notes and references

1 J. Yang, Z. Zhao, S. Wang, Y. Guo and Y. Liu, *Chem*, 2018, **4**, 2748–2785.
2 S. Fratini, M. Nikolka, A. Salleo, G. Schweicher and H. Sirringhaus, *Nat. Mater.*, 2020, **19**, 491–502.
3 X. Guo and A. Facchetti, *Nat. Mater.*, 2020, **19**, 922–928.
4 M. Ashizawa, Y. Zheng, H. Tran and Z. Bao, *Prog. Polym. Sci.*, 2020, **100**, 101181.
5 Y. Wang and T. Michinobu, *J. Mater. Chem. C*, 2018, **6**, 10390–10410.
6 H. Sun, X. Guo and A. Facchetti, *Chem*, 2020, **6**, 1310–1326.
7 H. Jia and T. Lei, *J. Mater. Chem. C*, 2019, **7**, 12809–12821.
8 S. Griggs, A. Marks, H. Bristow and I. McCulloch, *J. Mater. Chem. C*, 2021, **9**, 8099–8128.
9 K. Feng, H. Guo, H. Sun and X. Guo, *Acc. Chem. Res.*, 2021, **54**, 3804–3817.
10 P. Kafourou, B. Park, J. Luke, L. Tan, J. Panidi, F. Glöcklhofer, J. Kim, T. D. Anthopoulos, J.-S. Kim, K. Lee, S. Kwon and M. Heeney, *Angew. Chem., Int. Ed.*, 2021, **60**, 5970–5977.
11 Y. Wang, T. Hasegawa, H. Matsumoto and T. Michinobu, *J. Am. Chem. Soc.*, 2019, **141**, 3566–3575.
12 T. Hodsden, K. J. Thorley, J. Panidi, A. Basu, A. V. Marsh, H. Dai, A. J. P. White, C. Wang, W. Mitchell, F. Glöcklhofer, T. D. Anthopoulos and M. Heeney, *Adv. Funct. Mater.*, 2020, **30**, 2000325.
13 Y. Sui, Y. Deng, T. Du, Y. Shi and Y. Geng, *Mater. Chem. Front.*, 2019, **3**, 1932–1951.
14 Z. Zhao, Z. Yin, H. Chen, L. Zheng, C. Zhu, L. Zhang, S. Tan, H. Wang, Y. Guo, Q. Tang and Y. Liu, *Adv. Mater.*, 2017, **29**, 1602410.
15 M. Yang, T. Du, X. Zhao, X. Huang, L. Pan, S. Pang, H. Tang, Z. Peng, L. Ye, Y. Deng, M. Sun, C. Duan, F. Huang and Y. Cao, *Sci. China: Chem.*, 2021, **64**, 1219–1227.
16 T. Lei, J.-Y. Wang and J. Pei, *Acc. Chem. Res.*, 2014, **47**, 1117–1126.
17 E. Wang, W. Mammo and M. R. Andersson, *Adv. Mater.*, 2014, **26**, 1801–1826.

18 Z. Wang, Y. Shi, Y. Deng, Y. Han and Y. Geng, *Adv. Funct. Mater.*, 2021, **31**, 2104881.
19 C. Dong, S. Deng, B. Meng, J. Liu and L. Wang, *Angew. Chem., Int. Ed.*, 2021, **60**, 16184–16190.
20 Y. Sun, Y. Guo and Y. Liu, *Mater. Sci. Eng., R*, 2019, **136**, 13–26.
21 K. Guo, J. Bai, Y. Jiang, Z. Wang, Y. Sui, Y. Deng, Y. Han, H. Tian and Y. Geng, *Adv. Funct. Mater.*, 2018, **28**, 1801097.
22 Y. Shi, H. Guo, J. Huang, X. Zhang, Z. Wu, K. Yang, Y. Zhang, K. Feng, H. Y. Woo, R. P. Ortiz, M. Zhou and X. Guo, *Angew. Chem., Int. Ed.*, 2020, **59**, 14449–14457.
23 H. S. Kim, G. Huseynova, Y.-Y. Noh and D.-H. Hwang, *Macromolecules*, 2017, **50**, 7550–7558.
24 Y. Sui, Y. Deng, Y. Han, J. Zhang, W. Hu and Y. Geng, *J. Mater. Chem. C*, 2018, **6**, 12896–12903.
25 B. Fu, C.-Y. Wang, B. D. Rose, Y. Jiang, M. Chang, P.-H. Chu, Z. Yuan, C. Fuentes-Hernandez, B. Kippelen, J.-L. Brédas, D. M. Collard and E. Reichmanis, *Chem. Mater.*, 2015, **27**, 2928–2937.
26 S. Ma, G. Zhang, F. Wang, Y. Dai, H. Lu, L. Qiu, Y. Ding and K. Cho, *Macromolecules*, 2018, **51**, 5704–5712.
27 Z. Yuan, C. Buckley, S. Thomas, G. Zhang, I. Bargigia, G. Wang, B. Fu, C. Silva, J.-L. Brédas and E. Reichmanis, *Macromolecules*, 2018, **51**, 7320–7328.
28 L. Zhang, Z. Wang, C. Duan, Z. Wang, Y. Deng, J. Xu, F. Huang and Y. Cao, *Chem. Mater.*, 2018, **30**, 8343–8351.
29 Y. Wang, Z. Yan, H. Guo, M. A. Uddin, S. Ling, X. Zhou, H. Su, J. Dai, H. Y. Woo and X. Guo, *Angew. Chem., Int. Ed.*, 2017, **56**, 15304–15308.
30 J. Chen, X. Zhang, G. Wang, M. A. Uddin, Y. Tang, Y. Wang, Q. Liao, A. Facchetti, T. J. Marks and X. Guo, *J. Mater. Chem. C*, 2017, **5**, 9559–9569.
31 F. Wang, Y. Dai, W. Wang, H. Lu, L. Qiu, Y. Ding and G. Zhang, *Chem. Mater.*, 2018, **30**, 5451–5459.
32 Y. Sui, Y. Shi, Y. Deng, R. Li, J. Bai, Z. Wang, Y. Dang, Y. Han, N. Kirby, L. Ye and Y. Geng, *Macromolecules*, 2020, **53**, 10147–10154.
33 Y. Ran, Y. Guo and Y. Liu, *Mater. Horiz.*, 2020, **7**, 1955–1970.
34 J.-R. Pouliot, F. Grenier, J. T. Blaskovits, S. Beaupré and M. Leclerc, *Chem. Rev.*, 2016, **116**, 14225–14274.
35 J. Kuwabara, T. Yasuda, S. J. Choi, W. Lu, K. Yamazaki, S. Kagaya, L. Han and T. Kanbara, *Adv. Funct. Mater.*, 2014, **24**, 3226–3233.
36 M. Wakioka and F. Ozawa, *Asian. J. Org. Chem.*, 2018, **7**, 1206–1216.
37 N. S. Gobalasingham and B. C. Thompson, *Prog. Polym. Sci.*, 2018, **83**, 135–201.
38 S. Phan and C. K. Luscombe, *Trends Chem.*, 2019, **1**, 670–681.
39 P.-O. Morin, T. Bura and M. Leclerc, *Mater. Horiz.*, 2016, **3**, 11–20.
40 A. E. Rudenko and B. C. Thompson, *J. Polym. Sci., Part A: Polym. Chem.*, 2015, **53**, 135–147.
41 T. Bura, S. Beaupré, M.-A. Légaré, J. Quinn, E. Rochette, J. T. Blaskovits, F.-G. Fontaine, A. Pron, Y. Li and M. Leclerc, *Chem. Sci.*, 2017, **8**, 3913–3925.
42 T. J. Aldrich, A. S. Dudnik, N. D. Eastham, E. F. Manley, L. X. Chen, R. P. H. Chang, F. S. Melkonyan, A. Facchetti and T. J. Marks, *Macromolecules*, 2018, **51**, 9140–9155.
43 A. S. Dudnik, T. J. Aldrich, N. D. Eastham, R. P. H. Chang, A. Facchetti and T. J. Marks, *J. Am. Chem. Soc.*, 2016, **138**, 15699–15709.
44 T. Bura, S. Beaupré, O. A. Ibraikulov, M.-A. Légaré, J. Quinn, P. Lévêque, T. Heiser, Y. Li, N. Leclerc and M. Leclerc, *Macromolecules*, 2017, **50**, 7080–7090.
45 J. F. Ponder Jr, H. Chen, A. M. T. Luci, S. Moro, M. Turano, A. L. Hobson, G. S. Collier, L. M. A. Perdigão, M. Moser, W. Zhang, G. Costantini, J. R. Reynolds and I. McCulloch, *ACS Mater. Lett.*, 2021, **3**, 1503–1512.
46 A. Luzio, D. Fazzi, F. Nübling, R. Matsidik, A. Straub, H. Komber, E. Giussani, S. E. Watkins, M. Barbatti, W. Thiel, E. Gann, L. Thomsen, C. R. McNeill, M. Caironi and M. Sommer, *Chem. Mater.*, 2014, **26**, 6233–6240.
47 R. Matsidik, H. Komber, A. Luzio, M. Caironi and M. Sommer, *J. Am. Chem. Soc.*, 2015, **137**, 6705–6711.
48 S. Broll, F. Nübling, A. Luzio, D. Lentzas, H. Komber, M. Caironi and M. Sommer, *Macromolecules*, 2015, **48**, 7481–7488.
49 J.-R. Pouliot, B. Sun, M. Leduc, A. Najari, Y. Li and M. Leclerc, *Polym. Chem.*, 2015, **6**, 278–282.
50 D. Adamczak, B. Passarella, H. Komber, D. Becker-Koch, O. Dolynchuk, S. B. Schmidt, Y. Vaynzof, M. Caironi and M. Sommer, *Mater. Adv.*, 2021, **2**, 7881–7890.
51 Q. Wang, S. V. Lenjani, O. Dolynchuk, A. D. Scaccabarozzi, H. Komber, Y. Guo, F. Günther, S. Gemming, R. Magerle, M. Caironi and M. Sommer, *Chem. Mater.*, 2021, **33**, 668–677.
52 R. Matsidik, M. Giorgio, A. Luzio, M. Caironi, H. Komber and M. Sommer, *Eur. J. Org. Chem.*, 2018, 6121–6126.
53 Y. Gao, X. Zhang, H. Tian, J. Zhang, D. Yan, Y. Geng and F. Wang, *Adv. Mater.*, 2015, **27**, 6753–6759.
54 Y. Gao, Y. Deng, H. Tian, J. Zhang, D. Yan, Y. Geng and F. Wang, *Adv. Mater.*, 2017, **29**, 1606217.
55 K. Guo, Y. Jiang, Y. Sui, Y.-F. Deng and Y.-H. Geng, *Chin. J. Polym. Sci.*, 2019, **37**, 1099–1104.
56 Y. Gao, J. Bai, Y. Sui, Y. Han, Y. Deng, H. Tian, Y. Geng and F. Wang, *Macromolecules*, 2018, **51**, 8752–8760.
57 H. Sun, B. Liu, Y. Ma, J.-W. Lee, J. Yang, J. Wang, Y. Li, B. Li, K. Feng, Y. Shi, B. Zhang, D. Han, H. Meng, L. Niu, B. J. Kim, Q. Zheng and X. Guo, *Adv. Mater.*, 2021, **33**, 2102635.
58 Y. Shi, H. Guo, M. Qin, Y. Wang, J. Zhao, H. Sun, H. Wang, Y. Wang, X. Zhou, A. Facchetti, X. Lu, M. Zhou and X. Guo, *Chem. Mater.*, 2018, **30**, 7988–8001.
59 J. Yang, H. Wang, J. Chen, J. Huang, Y. Jiang, J. Zhang, L. Shi, Y. Sun, Z. Wei, G. Yu, Y. Guo, S. Wang and Y. Liu, *Adv. Mater.*, 2017, **29**, 1606162.
60 L. Xu, Z. Zhao, M. Xiao, J. Yang, J. Xiao, Z. Yi, S. Wang and Y. Liu, *ACS Appl. Mater. Interfaces*, 2017, **9**, 40549–40555.
61 N. M. Randell, C. L. Radford, J. Yang, J. Quinn, D. Hou, Y. Li and T. L. Kelly, *Chem. Mater.*, 2018, **30**, 4864–4873.
62 F. Chen, Y. Jiang, Y. Sui, J. Zhang, H. Tian, Y. Han, Y. Deng, W. Hu and Y. Geng, *Macromolecules*, 2018, **51**, 8652–8661.
63 J. A. Letizia, M. R. Salata, C. M. Tribout, A. Facchetti, M. A. Ratner and T. J. Marks, *J. Am. Chem. Soc.*, 2008, **130**, 9679–9694.
64 T. Lei, J.-H. Dou, X.-Y. Cao, J.-Y. Wang and J. Pei, *J. Am. Chem. Soc.*, 2013, **135**, 12168–12171.

65 N. E. Jackson, B. M. Savoie, K. L. Kohlstedt, M. Olvera de la Cruz, G. C. Schatz, L. X. Chen and M. A. Ratner, *J. Am. Chem. Soc.*, 2013, **135**, 10475–10483.
66 N. Zhou, X. Guo, R. P. Ortiz, S. Li, S. Zhang, R. P. H. Chang, A. Facchetti and T. J. Marks, *Adv. Mater.*, 2012, **24**, 2242–2248.
67 X. Zhou, N. Ai, Z.-H. Guo, F.-D. Zhuang, Y.-S. Jiang, J.-Y. Wang and J. Pei, *Chem. Mater.*, 2015, **27**, 1815–1820.
68 X. Guo, R. P. Ortiz, Y. Zheng, Y. Hu, Y.-Y. Noh, K.-J. Baeg, A. Facchetti and T. J. Marks, *J. Am. Chem. Soc.*, 2011, **133**, 1405–1418.
69 S. Shi, Y. Wang, M. A. Uddin, X. Zhou, H. Guo, Q. Liao, X. Zhu, X. Cheng, H. Y. Woo and X. Guo, *Adv. Electron. Mater.*, 2017, **3**, 1700100.
70 J. Bai, Y. Jiang, Z. Wang, Y. Sui, Y. Deng, Y. Han and Y. Geng, *Adv. Electron. Mater.*, 2020, **6**, 1901002.
71 Y. Zhou, C. Fuentes-Hernandez, J. Shim, J. Meyer, A. J. Giordano, H. Li, P. Winget, T. Papadopoulos, H. Cheun, J. Kim, M. Fenoll, A. Dindar, W. Haske, E. Najafabadi, T. M. Khan, H. Sojoudi, S. Barlow, S. Graham, J.-L. Brédas, S. R. Marder, A. Kahn and B. Kippelen, *Science*, 2012, **336**, 327–332.
72 A. D. Scaccabarozzi, A. Basu, F. Aniés, J. Liu, O. Zapata-Arteaga, R. Warren, Y. Firdaus, M. I. Nugraha, Y. Lin, M. Campoy-Quiles, N. Koch, C. Müller, L. Tsetseris, M. Heeney and T. D. Anthopoulos, *Chem. Rev.*, 2022, **122**, 4420–4492.
73 I. McCulloch, A. Salleo and M. Chabinyc, *Science*, 2016, **352**, 1521–1522.
74 H. H. Choi, K. Cho, C. D. Frisbie, H. Sirringhaus and V. Podzorov, *Nat. Mater.*, 2018, **17**, 2–7.
75 J. Mei, D. H. Kim, A. L. Ayzner, M. F. Toney and Z. Bao, *J. Am. Chem. Soc.*, 2011, **133**, 20130–20133.
76 S. Park, M. H. Lee, K. S. Ahn, H. H. Choi, J. Shin, J. Xu, J. Mei, K. Cho, Z. Bao, D. R. Lee, M. S. Kang and D. H. Kim, *Adv. Funct. Mater.*, 2016, **26**, 4627–4634.
77 J. Lee, A. R. Han, H. Yu, T. J. Shin, C. Yang and J. H. Oh, *J. Am. Chem. Soc.*, 2013, **135**, 9540–9547.
78 D.-H. Lim, Y.-J. Kim, Y.-A. Kim, K. Hwang, J.-J. Park and D.-Y. Kim, *Chem. Mater.*, 2019, **31**, 4629–4638.

